

Partial decomposition of TiH₂ studied in situ by ED-XRD and ex situ by XRD- μ CT using hard X-ray synchrotron radiation

C. Jiménez^{1,2}, F. Garcia-Moreno^{1,2}, B. Pfretzschner^{1,2}, A. Rack³, R. Tucoulou³,
T. Rack⁴, P. Cloetens³, M. Klaus², J. Banhart^{1,2}

¹ Technische Universität Berlin, Hardenbergstr. 36, 10623 Berlin, Germany

² Helmholtz-Zentrum Berlin für Materialien und Energie, Hahn-Meitner-Platz 1,
14109 Berlin, Germany

³ European Synchrotron Radiation Facility, BP 220, 38043 Grenoble, France

⁴ Charité Berlin, Charitéplatz 1, 10117 Berlin, Germany

ABSTRACT

The phase transformations of TiH₂ during its partial decomposition were followed in situ by ED-XRD and compared to thermoanalytical traces. During *heating* up to 616 ± 5 °C, endothermic peaks of H₂ release accompanied by mass loss, are correlated with individual phase transformations and the phases $\alpha+\delta+\beta$ co-exist. During *cooling* no further mass loss occurs, which suppresses the co-existence of $\alpha+\delta+\beta$, and the transformation $\alpha + \beta \xrightarrow{232 \pm 7^\circ\text{C}} \alpha + \delta$ takes place along with an exothermic peak. After cooling ED-XRD and XRD- μ CT revealed a heterogeneous distribution of δ lamellae embedded in an α matrix inside the powder particles in proportions 30:70 (vol. %).

Introduction

TiH₂ powder can be used for foaming low melting Al- [Garc04, Garc09], Zn- [Kita06, Garc10Zn] or Mg-based [Bach05] alloys. As-received TiH₂ powder is commonly admixed to a metal powder mixture in fractions of 0.5 to 2 wt.%, after which the blend is hot-consolidated and subsequently foamed by heating. As the alloy melts, TiH₂ decomposes, thereby releasing H₂ gas that creates bubbles [Baum00]. The decomposition of TiH₂ is therefore important to understand. Precursors are heated up to temperatures sufficient to melt the alloy – 430 to 650 °C for the examples mentioned – and to initiate H₂ release. Isochronal decomposition of as-received TiH₂ powder takes place in various stages in which H₂ release peaks. The stages are correlated to phase transformations in TiH₂, start at about 370-380 °C and end at about 950 °C [Matl06, Liu010, Jime11]. During foaming, however, decomposition is

mostly interrupted. The associated partial decomposition of TiH₂ has been studied ex-situ by X-ray diffraction [Borc09] but not yet in-situ. Thus, understanding partial decomposition of TiH₂ is important to further improve metal foam manufacture.

For this study, we followed in-situ the phase transformations of TiH₂ powder and compared them to thermoanalytical traces obtained under equal temperature and atmospheric conditions. We quantified volume fractions of phases after partial decomposition and determined non-destructively their spatial distribution inside single particles with sub- μm resolution by using scanning X-ray tomography with powder diffraction-based contrast (XRD- μCT) [Bleu08, Stoc08].

Experiments

As-received TiH₂ powder (supplied by Chemetall GmbH, Frankfurt, particle size < 36 μm) was both heated and cooled under flowing Ar. The phase transformations were followed in-situ by ED-XRD at the EDDI experimental station hosted at the synchrotron facility BESSY II of the Helmholtz Centre Berlin [Genz07]. We illuminated the samples with a white beam of X-rays and the energy of diffracted photons was measured in transmission at a fixed $2\theta = 8^\circ$ by a multi-channel analysing detector. Powder samples were poured into an alumina crucible of 5 mm diameter. We inserted a thermocouple through a hole in the crucible wall for measuring the sample temperature T_s . The crucible was tightened to the heating plate of an Anton Paar DHS 1100 furnace. A second thermocouple measured the heater temperature T_H . A thin graphite dome closed the furnace chamber. After evacuation and backfill with Ar gas, a gas pressure of 1.2 bar at the inlet induced Ar flow through the chamber. The heater temperature was increased from 30 to 680 $^\circ\text{C}$ at 10 $\text{K}\cdot\text{min}^{-1}$. Following the heater was turned off and natural cooling took place. One spectrum was acquired every 12.4 s. Additional spectra were acquired for 60 s after cooling for quantitative phase analysis.

Simultaneous thermogravimetry and mass spectroscopy (TG-MS) were conducted in a Netzsch 209 C thermobalance coupled via a capillary to a quadrupole mass spectrometer QMS 209. We poured 90 mg of TiH₂ powder into an alumina crucible. Samples were heated at 10 $\text{K}\cdot\text{min}^{-1}$ from 35 to 620 $^\circ\text{C}$ and cooled at 40 $\text{K}\cdot\text{min}^{-1}$ under flowing Ar atmosphere. Differential scanning calorimetry (DSC)

was done in a Netzsch STA 204 C applying identical temperature profile and atmosphere as for TG-MS.

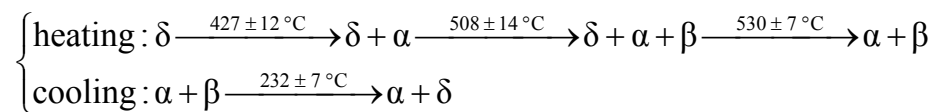
The spatial distribution of phases inside individual particles was characterised non-destructively after ED-XRD by scanning X-ray microtomography at the nano-station ID22NI of the European Synchrotron Radiation Facility [Mart11]. ID22NI was operated in monochromatic mode (17.5 keV photon energy). The X-rays were focused by multilayer-coated KB-optics to a spot size of 140 nm × 200 nm (h × v, FWHM). Tomographic scans were performed by scanning lines of the slice of interest horizontally (150 points, 260 nm step size), then rotated by 3°, and scanned again until a 180° rotation was completed. For each point of the scans, the powder diffraction pattern was collected. The software package XRDUa was employed for data processing [Nolf10]. Additionally, the sample was scanned using full-field microtomography at the ESRF beamline ID19 (0.3 μm pixel size, 17.6 keV).

Further microstructural characterisation was done by scanning electron microscopy (SEM) in a Zeiss SUPRA VP operated at 10 kV accelerating voltage. For this, the powders were mixed with an epoxy resin and cast. After curing, samples were ground and polished.

Results

Fig. 1 a shows the density map of diffraction intensities dispersed in energies as function of time obtained while heating and cooling the TiH₂ powder under flowing Ar. The profiles $T_H(t)$ and $T_S(t)$ depart from one another with increasing temperature because heat conduction through the powder sample becomes poorer. Temperatures linked to diffraction lines come from $T_S(t)$. Temperatures of individual transformations are average values from different samples.

The starting phase δ belongs to the cubic space group (s.g.) $Fm\bar{3}m$, in which Ti atoms form a fcc sublattice and H atoms sit on tetrahedral sites [SanM87]. As temperature increases the two hydrogen solid solutions α and β appear. α is hcp (s.g. $P6_3mmc$), β bcc (s.g. $Im\bar{3}m$) and in both, H atoms randomly occupy tetrahedral sites [SanM87]. According to Fig. 1 a, the phase transformation sequence is:



Sequential fittings for the diffraction lines δ_{220} , δ_{200} , α_{101} , α_{102} and β_{200} render $E_{i_{hkl}}$ values which via Bragg's law yield $d_{i_{hkl}}$ values and, from these, lattice parameters [Cull78] whose time and temperature dependence is given in Fig. 1 b. Details of the calculations are given in Supplement A. During heating, a_δ expands linearly up to 373 ± 5 °C. After this, a_δ contracts until δ vanishes. The lattice parameters a_β and c_α also decrease during heating, whereas a_α remains fairly constant. During cooling, both c_α and a_α contract continuously but a_β expands below 497 ± 15 °C. When a_β vanishes at 232 ± 7 °C, a_δ reappears and fluctuates around 4.405 Å.

The evolution of integrated intensities $I_{i_{hkl}}$ ($i = \alpha, \beta$ or δ) with time and temperature for the diffraction lines δ_{200} , α_{101} and β_{200} , is also presented in Fig. 1 b. They are proportional to the evolution of corresponding volume fractions f_{vi} of the phases [Lain78].

Analysis of the ED diffraction spectrum after cooling yields volume fractions $V_\alpha = 68.9\%$ and $V_\delta = 31.1\%$ with standard deviations of 3.3% using the intensities $I_{i_{hkl}}$ of the peaks marked by arrows in Fig. 1 c, bottom and Supplement A [Lain78]. This spectrum obtained at EDDI corresponds to a powder sample containing a large number of particles, whereas the diffractogram obtained at ID22NI (also given in Fig. 1 c) is the summed pattern of the whole XRD- μ CT scanned section inside a cluster of just a few particles. Both patterns are in good agreement. Fig. 2 a1 depicts the size and morphology of the scanned particle cluster. Fig. 2 a2 represents the XRD- μ CT reconstruction of the scanned section using the complete pattern given in Fig. 1 c, top. In this reconstruction the phases α and δ are not distinguishable, but the complex geometry of the particles and their variable sizes are visible. Fig. 2 a3 and a4 show individual spatial distributions of α and δ in the scanned section. Both phases are heterogeneously distributed and α occupies a larger area of the section than δ . Fig. 2 a5 is the combined map of both α and δ in which δ -rich regions appear surrounded by or adjacent to wider α -rich areas (see e.g. encircled region).

The microstructural analysis conducted by SEM is given in Fig. 2 b. The microstructure comprises a heterogeneous distribution of bright both coarse and thin lamellae, indicated as **cL** and **tL** respectively, embedded in a darker matrix **M**. The inset contains an enlargement to show that **tL** are often parallel to each other, have clearer orientation and flatter boundaries with respect to the matrix than **cL**.

TG-MS and DSC traces are summarized in Fig. 3. The mass = 2 ion current $I_{m=2}$ is an instantaneous measure of the H₂ gas release and is proportional to the mass change rate, i.e. $I_{m=2} \propto -\partial(\Delta m)/\partial t$ [Matl06]. The H₂ gas release starts at 380 °C, has a multi-peak structure during heating and decays fast when cooling starts. The mass change Δm reached -2.6 % during heating and remained fairly constant upon cooling. The heat flow trace resembles $I_{m=2}$ during heating as expected [Matl06], but has a distinctive exothermic peak with onset at 230 °C during cooling.

4. Discussion

4.1 Co-existence of $\alpha+\beta+\delta$ on heating suppressed on cooling by mass conservation

As recently reported, during heating under Ar flow, every endothermic peak of H₂ release and the associated mass loss is correlated with contraction regimes of lattice parameters [Jime11]. Dehydrogenation accompanied by mass loss starts when the lattice parameter a_δ starts to contract at 375 ± 5 °C (see a_δ in Fig. 1 b and onset temperature 380 °C in Fig. 3). We clarified in that work and confirm in the present one that the removal of H₂ gas by Ar flow favours the formation and persistence of an α -shell around a δ/β -core because α has the lowest H solubility S_H^α (see Fig. 4) and therefore, is the phase most compatible with the atmosphere [Jime11]. In such a core-shell structure there is a hydrogen concentration C_H gradient within the particles – C_H is lower at the surface in the α shell than in the δ/β core. This is linked to the H solubility ranking for the three phases $S_H^\alpha < S_H^\beta < S_H^\delta$ as inferred from Fig. 4 [Jime11]. This C_H gradient enables the co-existence of $\alpha+\beta+\delta$ which otherwise would not be possible in the eutectoid Ti-H system given in Fig. 4 [Matl06, Lui010, Jime11].

For complete dehydrogenation, α is the final phase and no transformation occurs during cooling [Lui010, Jime11]. There is no phase transformation either if cooling starts from lower temperatures in which there is only $\alpha+\delta$, i.e. before β appears (Supplement B). In the present work, we start cooling from 616 ± 5 °C when β is the predominant phase (Fig. 1 b). From this condition the phase transformation $\alpha + \beta \xrightarrow{232 \pm 7^\circ\text{C}} \alpha + \delta$ takes place because in the Ti-H system β cannot be retained by natural cooling or water quenching [Borc09]. This transformation contains the eutectoid reaction $\beta \rightarrow \alpha+\delta$ which is shifted by -70 K with respect to the equilibrium

temperature of 300°C due to continuous cooling at 40 K·min⁻¹ [SanM87] and is correlated with the exothermic peak shown in Fig. 3.

In principle, we could describe the cooling path by dropping an arrow from 616 °C for the remaining 1.2 wt.% H (3.8 (total) – 2.6 (mass loss) = 1.2) as done in Fig. 4. If the sample were in equilibrium at 616 °C, only β should be present, but in reality, when cooling starts α+β is found due to the stabilization of α by continuous hydrogen removal through Ar flow [Jime11]. This is one of the reasons why the resulting α:δ ratio is 75:25 (in wt.%, equivalent to 70:30 in vol.%) instead of the theoretical 60:40 inferred from the Ti-H phase diagram for C_H of 1.2 wt.% H as indicated in Fig. 4.

Despite the fact that the cooling rate is 4 times higher than the heating rate at around 232 °C, mass conservation suppresses the C_H gradient and thus the co-existence of α+β+δ, as one would expect from the cooling path indicated in Fig. 4. The uncertainty for the transformation temperature 232 ± 7 °C originates from the scatter between measurements, but all individual measurements show no co-existence of α+β+δ during cooling as in Fig. 1a and b (see analogous to Fig. 1a but for another sample in Supplement C).

4.2 Evolution of lattice parameters and volume fractions of phases on cooling

The cooling path in Fig. 4 helps understanding the evolution of volume fractions and lattice parameters of phases as temperature decreases for this slightly hypoeutectoid composition. Just before cooling started at 616 ± 5 °C, f_{vβ} reached its maximum and f_{vα} a local minimum (see Fig. 1b). As temperature decreases, f_{vα} increases and f_{vβ} decreases, indicating that the sample behaves as if it were in the α+β field. This effect is attributed to the 1.37 wt.% oxygen content in this commercial powder [Jime11], which is known to enlarge the α+β field as indicated in Fig. 4 [Müll68]. Inside the α+β field, β enriches in H because f_{vα} increases and f_{vβ} decreases, but C_H is constant and also, the hydrogen solubility in β increases up to the eutectoid composition whereas the solubility of α decreases below 600 °C [SanM87]. Due to this H enrichment a_β expands below 497 ± 15 °C whereas a_α and c_α shrink continuously due to temperature and solubility reduction. The sudden transformation α + β $\xrightarrow{232 \pm 7 \text{ }^\circ\text{C}}$ α + δ involves also a quick and substantial increase of f_{vα} which

subsequently reaches a maximum value. $f_{v\delta}$ remains fairly constant since it reappears as expected after entering the $\alpha+\delta$ field.

4.3 Spatial distribution of phases after cooling

A comparison between Fig. 2 a5 and Fig. 2 b, considering that the volumes are related like $\alpha:\delta = 70:30$, indicates that in the resulting microstructure the matrix is α and the lamellae are δ . In the core-shell model proposed in Ref. Jime11 for an average particle of 6 μm diameter, α would occupy a shell of about 0.2 μm thickness at 616 $^{\circ}\text{C}$ and cover a β core. TEM investigations showed that such core-shell structures can be retained after cooling down from 430 $^{\circ}\text{C}$, i.e. from the $\alpha+\delta$ field, because no phase transformation is involved during cooling. But cooling down from 616 $^{\circ}\text{C}$ involves the eutectoid transformation of β in most of the particle volume. This prevents a high temperature core-shell structure to be retained, thus leading to the resulting heterogeneous distribution of α and δ in which cL precipitate before tL and therefore, grow and lose interfacial coherence with respect to the matrix [Port81]. If such a core-shell distribution of phases after cooling existed, the non-destructive XRD- μCT analysis would certainly have detected it, as similar studies suggest [Moch11], but no such observation was made.

5 Summary

During *heating*, endothermic peaks and their associated mass changes are correlated with individual phase transformations and regimes of lattice parameter contraction. Simultaneous temperature increase and H_2 removal by flowing Ar creates a hydrogen concentration gradient inside the particles and a core-shell structure of phases in which $\alpha+\delta+\beta$ co-exist. When *cooling* starts at 616 ± 5 $^{\circ}\text{C}$, there is no further mass loss and the phase transformation $\alpha + \beta \xrightarrow{232 \pm 7^{\circ}\text{C}} \alpha + \delta$ is correlated with an exothermic peak. Due to mass conservation and the large volume fraction β occupies before cooling starts, the co-existence of $\alpha+\delta+\beta$ is suppressed. No evidence of an existing α -shell/ β -core at high temperatures remains and the resulting microstructure is a heterogeneous distribution of δ -lamellae embedded in an α -matrix in volume proportions $\alpha:\delta = 70:30$.

References

- [Bach05] Fr.-W. Bach, D. Bormann, P. Wilk, R. Kucharski, Cellular Metals and Polymers, Eds.: R.F. Singer, C. Körner, V. Altstadt, H. Münster, Trans Tech Publications, Zürich, 2005, 77.
- [Baum00] J. Baumeister, German Patent DE40 18 360, 1990.
- [Bleu08] P. Bleu, E. Welcomme, E. Dooryhée, J. Susini, J.-L. Hodeau, Ph. Walter, Nature Materials 2008, 7, 468.
- [Broc09] Ch. Borchers, T.I. Khomenko, A.V. Leonov, O.S. Morozova, Thermochim Acta 2009, 493, 80.
- [Chet10] A. Chethan, F. Garcia-Moreno, N. Wanderka, B.S. Murty, J. Banhart, J Mater Sci. (in print) doi 10.1007/s10853-011-5761-8
- [Garc04] F. Garcia-Moreno, M. Fromme, J. Banhart, Adv. Eng. Mater. 2004, 6, 416.
- [Garc09] F. Garcia-Moreno, C. Jiménez, M. Mukherjee, P. Holm, J. Weise, J. Banhart, Colloids and Surfaces A, 2009, 344, 101.
- [Genz08] Ch. Genzel, I. Denks, J. Gibmeier, M. Klaus, G. Wagener, Nucl Instr and Meth in Phys Res A 2007, 578, 23.
- [Jime11] C. Jiménez, F. Garcia-Moreno, B. Pfretzschner, M. Klaus, M. Wollgarten, I. Zizak, G. Schumacher, M. Tovar, J. Banhart, Acta Mater 2011, 56, 6318.
- [Kita06] K. Kitazono, Y. Takiguchi, Scripta Mater. 2006, 55, 501.
- [Liu010] H. Liu, P. He, J.C. Feng, J Cao. Int J Hydrogen Energy 2010; 34: 3018.
- [Mart11] G. Martinez-Criado, R. Tucoulou, P. Cloetens, P. Bleu, Synchrotron Radiat 2011, submitted.
- [Matl06] B. Matijasevic-Lux, J. Banhart, S. Fiechter, O. Görke, N. Wanderka, Acta Mater 2006; 54: 1887.
- [Moch11] C. Mochales, A. Maerten, A. Rack, P. Cloetens, W.D. Mueller, P. Zaslansky, C. Fleck, Acta Biomater. 2011, 7, 2994.
- [Müll68] W.M. Müller. *Titanium Hydrides*, in: W.M. Müller, Blackledge JP, G.G. Libowitz (Eds.). Metal Hydrides. New York: Academic Press; 1968.
- [Nolf10] W. De Nolf and K. Janssens, Surf. Interface Anal., 2010, 42, 411.
- [Port81] K.E. Easterling, Phase Transformations in Metals and Alloys. London: Chapman and Hall; 1981
- [SanM87] A. San Martin, F.D. Manchester. Bull Alloy Phase Diag 1987; 8: 30.
- [Stoc08] S.R. Stock, F. De Carlo, J.D. Almer, J Struct. Biol. 2008, 161, 144.

Figure captions

Fig. 1a – Density map of diffracted intensities dispersed in energies given as function of time. The evolution of the phases δ , β and α during heating and cooling under Ar flow is shown. Number triples are hkl indices. Temperatures come from $T_S(t)$. **b** – Evolution of lattice parameters and integrated intensities and $T_S(t)$. **c** – Diffractograms obtained after cooling at the instruments EDDI and ID22NI.

Fig. 2 – Top: **a1** – Microtomogram of the scanned particle cluster. **a2** – XRD- μ CT reconstruction based on the entire diffraction pattern given in **Fig. 1 c**. Bottom: spatial distributions of δ (**a3**) and α (**a4**) phases as well as the combination of both (**a5**). **b** – Microstructure of particles after cooling as seen by SEM.

Fig. 3 – Thermoanalytical DSC combined with gravimetric/mass-spectroscopic traces (Δm and $I_{m=2}$) of TiH_2 powders heated up to 620 °C and cooled down under Ar flow. Top: measured temperatures profiles $T_{\text{TG-MS}}(t)$ and $T_{\text{DSC}}(t)$.

Fig. 4 – Phase diagram of the Ti-H system [[SanM87](#)]. Lines extending the $\alpha+\beta$ field within 600-900 °C and 0-30 at.% H are taken from [[Müll68](#)]. Remaining H at 616 °C is 1.2 wt.%. The red arrow indicates the equilibrium cooling path.